Incorporation of chlorine in nuclear waste glasses using high-pressure vitrification: Solubility, speciation, and local environment of chlorine

Valentin Jolivet, Yann Morizet, Nicolas Trcera, Vincent Fernandez, Tomo Suzuki-Muresan

Incorporation of chlorine in nuclear waste glasses using high-pressure vitrification: Solubility, speciation and local environment of chlorine

Valentin JOLIVET[1,2,3], Yann MORIZET*[1], Nicolas TRCERA[4], Vincent FERNANDEZ[2], Tomo SUZUKI-MURESAN[3]

[1]Nantes Université, Univ. Angers, Le Mans Université, CNRS, UMR 6112, Laboratoire de Planétologie et Géosciences, F-44000 Nantes, France

[2]Nantes Université, CNRS, Institut des Matériaux de Nantes Jean Rouxel, IMN, F-44000 Nantes, France

[3]Nantes Université, IMT Atlantique, CNRS, SUBATECH, F-44000 Nantes, France

[4]Synchrotron SOLEIL, L'Orme des Merisiers, Saint Aubin, BP 48, F-91192 Gif-sur-Yvette Cedex, France

*Corresponding author: Yann Morizet

Postal address:

Laboratoire de Planétologie et Géosciences de Nantes (LPG Nantes), UMR-CNRS 6112, Université de Nantes.

2 rue de la Houssinière, 44322 Nantes Cedex (FRANCE)

phone: +33 (0) 2 5112 5491

fax: +33 (0) 2 5112 5268

*E-mail: yann.morizet@univ-nantes.fr

ABSTRACT

The solubility, speciation and local atomic environment of chlorine have been determined for aluminoborosilicate glasses quenched from high-pressure (0.5-1.5 GPa) and high-temperature (1350-1400°C) equilibrated with various sources of chlorine (NaCl and $PdCl_2$). The Cl solubility reaches up to 11 mol.% in borosilicate glass and appears to be strongly influenced by the concentration of network modifying cations (Ca and Na) and increases with increasing $CaO + Na_2O$ content. The Cl solubility is enhanced in Ca-bearing rather than Na-bearing borosilicate glass, suggesting a higher affinity of chlorine for alkaline-earth cations. Cl K-edge XANES and Cl 2p XPS spectra reveal that chlorine dissolves in glasses only as chloride species (Cl^-) and no evidence of oxidized species is observed. Using $PdCl_2$ as a chlorine starting source leads to pre-edge signal for $PdCl_2$ in the XANES spectra. The EXAFS simulations show that Cl^- local environment is charge compensated by Na^+ or Ca^{2+} at a distance to first neighbor on the order of 2.7 Å that is comparable to the observed distances in chlorine crystalline compounds. The coordination to charge compensating cation is lower in the case of Ca^{2+} (~1.1) than Na^+ (~4.3).

Keyword

High-pressure, Chlorine, Nuclear Waste Glasses, spectroscopy.

INTRODUCTION

^{36}Cl is a long-lived and radiotoxic radioisotope (301 ky, Endt and Van der Leun 1973, Audi et al. 2017) arising from irradiated graphite in nuclear reactors (Wickham et al. 2017). ^{36}Cl is found to be a major pollutant of ground water after the Chernobyl nuclear plant accident (Chant et al. 1996, Roux et al. 2014). ^{36}Cl is mixed with stable Cl during the pyrochemical

49 reprocessing of spent fuel (Metcalfe and Donald 2004, Tomilin et al. 2007, Vance et al. 2012,
50 Gin et al. 2017). The volatility of this element prevents its incorporation in common nuclear
51 waste glass formulations with usual vitrification process in melters at ambient pressure (see
52 Hrma 2010, Ilyukhina et al. 2010, Ojovan and Lee 2011, Gin et al. 2017, Goel et al. 2019).
53 This behavior at high-temperature is an important obstacle owing to the ^{36}Cl high mobility in
54 the environment, radiotoxicity and long half-life. Consequently, alternative processing should
55 be proposed for immobilizing in a safe and permanent manner the ^{36}Cl-bearing nuclear
56 wastes. Besides, it should be emphasized that ^{36}Cl is thought to be one of the main
57 contributors of the dose released from geological repositories such as the CIGEO project
58 (Meplan and Nuttin 2015). Therefore, the immobilization of chlorine is mostly dependent on
59 the conditioning matrix durability.
60 A great deal of effort has been spent these last decades to develop specific glass formulations
61 to increase chlorine retention in glasses, especially in the alkaline-earth silicate glass systems
62 (Siwadamrongpong et al. 2004, Schofield et al. 2009, Tan 2015, Chen et al. 2017, Tan and
63 Hand 2018, Zhao et al. 2019). Paradoxically, chlorine behavior in glasses is better known than
64 other halogen behavior such as iodine, even though ^{129}I is of more concern than ^{36}Cl for
65 geological disposal of nuclear wastes (Meplan and Nuttin 2015, Riley et al. 2016, Jolivet et al.
66 2020, 2021, Morizet et al. 2021a,b). It is due to the interest from the geological community
67 for chlorine, as it is an important volatile species involved in the degassing of the planetary
68 interior through magmatic processes (Johnston 1980, Symonds et al. 1988, Carroll 2005).
69 Indeed, chlorine has a great influence on magmatic processes such as diffusion, density and
70 viscosity; which are important to constrain for eruptive processes (Métrich and Rutherford
71 1992, Carroll and Webster 1994, Dingwell and Hess 1998, Aiuppa et al. 2004, Zimova and
72 Webb 2007, Evans et al. 2008, Aiuppa et al. 2009, Filiberto and Treiman 2009, Baasner et al.

2013, Dalou et al. 2015, Webster et al. 2015, 2018). These works use high-pressure and high-temperature conditions to increase the solubility of chlorine in melts to prevent evaporation, and to allow the understanding of the dependence of chlorine solubility as a function of chemical and physical parameters. For instance, it has been demonstrated that Cl solubility is strongly dependent on CaO content (Carrol and Webster 1994, Signorelli and Carroll 2002, Evans et al. 2008) and that Cl has strong structural affinities with Ca in glasses (McKeown et al. 2011). Cl solubility is negatively affected by the Al content (Dalou et al. 2015), which may be ascribed to a rivalry for the use of charge balancing cations, as observed for iodine (Jolivet et al. 2020, Morizet et al. 2021b).

Cl solubility in borosilicate glasses is not extensively investigated, as the actual industrial processes are inefficient for Cl retention in glasses at atmospheric pressure (Hrma 2010). The most interesting work yet regarding chlorine behavior in borosilicate glasses is the work by Tan (2015) and Tan and Hand (2018); the latter being limited to the aluminosilicate glass compositions. More recently, Zhao et al. (2019) focused mostly on the role of alkaline-earth cations for chlorine incorporation in glasses and concluded that i) Cl solubility in borosilicate glasses increased with the size of the alkaline-earth element, the highest Cl content (2.54 at.%) reached for a Ba-bearing borosilicate glass, ii) the same applied to aluminosilicate glasses, iii) glass composition seemed more important than melting temperature to incorporate Cl in glasses, iv) Cl decreased glass transition temperature in a comparable way to other halogens such as iodine (Jolivet et al. 2021) or fluorine (Zimova and Webb 2007), v) Cl affected the polymerization of the glass network, as for iodine (Jolivet et al. 2020), and vi) above chlorine saturation, phase separation occurred, but Cl was not necessarily present in the newly formed phase, neither was it retained in the glass. Although, the aforementioned studies constitute landmarked works in the race for the understanding of chlorine behavior and its

immobilization in specific glass matrices, the Cl contents reached in these nuclear waste glass could be drastically improved using pressurization vitrification. Vitrification at ambient pressure cannot prevent chlorine from escaping by evaporation, despite all the effort made to improve the process (Tan 2015, Tan and Hand 2018). Furthermore, high-pressure conditions may help to prevent phase separation, which seems to be a common issue when dealing with chlorine (see Tan 2015, Gin et al. 2017).

In the present work, we investigate the chlorine incorporation into glasses synthesized under high-pressure and high-temperature conditions. We explore borosilicate glasses with varied compositions to investigate the role of boron, the role of alkali and alkaline-earth contents in the Cl incorporation. The local atomic environment of Cl is also investigated using X-ray Photoelectron Spectroscopy (XPS) and X-ray Absorption Spectroscopy (XAS), in order to determine the impact of high-pressure conditions on the Cl environment in glasses. We also attempt to discuss the systematics of Cl solubility in glasses using a field strength formalism.

EXPERIMENTAL METHODS

Starting Material

We investigated chlorine solubility in various glass compositions in the system SiO_2-Al_2O_3-B_2O_3-CaO-Na_2O (-ZrO_2). Most of the compositions were synthesized in Jolivet et al. (2019, 2020, 2021) and Morizet et al. (2021a,b) to study the incorporation of iodine in glasses. The preparation of volatile-free glasses is described elsewhere (Jolivet et al. 2019). Glass batches were prepared from a mixture of oxides (SiO_2, Al_2O_3, CaO) and carbonates (Na_2CO_3). Prior to the high-pressure syntheses, these glasses were melted in a box furnace at 1200°C for 1 to 2 hours. Experiments on the ISG (International Simple Glass) composition were conducted from a provided ISG ingot that was also used as a standardized glass for nuclear waste glass

121 studies (see Gin et al. 2013). This glass has been intensively studied by the community
122 (Inagaki et al. 2013, 2014, Elia et al. 2017, Abdelouas et al. 2013, Charpentier et al. 2016,
123 Mendoza et al. 2012, Mohd et al. 2015, Guerette and Huang 2015, Collin et al. 2018, Jolivet
124 et al. 2019) including for investigations on iodine incorporation in glasses using extreme
125 conditions (Jolivet et al. 2020, 2021, Morizet et al. 2021b). All the studied glass compositions
126 and experimental conditions are provided in the Table 1.

127 The ISG, LJ8 and BASN3 compositions are polymerized glasses, with a high concentration of
128 network forming oxides (SiO_2, Al_2O_3, B_2O_3). The main difference between these glasses is
129 mostly represented by the change in the K* parameter defined as ($[SiO_2]+[Al_2O_3]$)/$[B_2O_3]$ and
130 modified after the K parameter from Dell et al. (1983). The ISG composition is an high silica
131 glass (60.2 mol.% SiO_2), with 16 mol.% B_2O_3 to ease the melting and optimize the physical
132 properties, and a small amount of Al_2O_3 and ZrO_2 stabilizing the network. The Na_2O and CaO
133 content are optimized to balance the charges of the AlO_4^- and ZrO_6^- units, and to have a
134 relatively high N_4 (~0.5, Charpentier et al. 2016, $N_4 = [BO_4] / [BO_4] + [BO_3]$, see Dell et al.
135 1983). The LJ8 composition is similar to the ISG composition, but with a lower B_2O_3 content
136 (6.4 mol.%, Jolivet et al. 2019), and slightly more Al_2O_3, CaO, and Na_2O. Consequently, the
137 K* of this glass, is higher than the K* of the ISG (10.8 vs 4, see Table 1). The BASN3
138 composition is even lower in B_2O_3 content (4.8 mol.%), and higher in SiO_2 and Al_2O_3 (64.6
139 and 9.8 mol.%, respectively). This glass has a higher K* than ISG and LJ8 (15.5), and the N_4
140 is 0.52 (see Jolivet et al. 2019). In BASN3, the Na_2O is the only non-network former (21.1
141 mol.% Na_2O, Table 1).

142 The other glasses of this study, NH, LJ4b, BFS3 and 4, C35, and the pCABS1 and 2, are
143 depolymerized glasses, featuring low network former oxide content and relatively high non-
144 network former content. The NH composition has been extensively used in Jolivet et al.

145 (2020, 2021) to investigate the effect of the incorporation of iodine in glasses. It is a
146 simplified simulant of LAW glasses (Low Activity Waste, see Ojovan and Lee 2011), with a
147 high Na_2O content (24.2 mol.%). It has a relatively low SiO_2 content (43.1 mol.%) and almost
148 the same B_2O_3 content as ISG (15.1 mol.%, Table 1) but with a higher Al_2O_3 content, so the
149 K* of NH is nearly identical to ISG (3.5 and 4, respectively). BFS3 and 4 are similar to NH,
150 but a part of the Na_2O content is substituted with CaO (see Table 1). The pCABS1 and 2
151 glasses are similar to NH, but do not contain Na_2O that is replaced by CaO. The pCABS1 has
152 a slightly different K* from pCABS2 (2.6 and 3.9, respectively) due to different B_2O_3 content
153 (substitution with CaO content, see Table 1). The C35 is a B_2O_3 rich glass (29.1 mol.%), that
154 does not contain Na_2O (33.6 mol.% CaO) and has been studied in Morizet et al. (2021a). It
155 has one of the lowest K* with LJ4b (1.3 and 1.5, respectively). LJ4b has an intermediate SiO_2
156 content (49.8 mol.%), an high B_2O_3 content (33.8 mol.%), and a high Na_2O content (16.4
157 mol.%, Table 1). The N_4 of this glass is 0.42 (in Jolivet et al. 2019). Overall, the investigated
158 glass compositions probe a large range of B_2O_3 (5-35 mol.%), large range of SiO_2 (30-65
159 mol.%) and a large range of network modifying cations (9-33 mol.%) with either CaO or
160 Na_2O or both as the nature of network modifying cation.

161 **High-pressure syntheses**

162 The experimental charge consists of a mix of glass powder (~300 mg) and a Cl-bearing
163 compound (~30 mg), such as NaCl or $PdCl_2$. The NaCl is dried at 500°C for 24 h in a box
164 furnace prior to loading. We also use $PdCl_2$ as Pd and Cl_2 dissociates at high-temperature, and
165 Pd is poorly soluble in glasses, as described in Dalou et al. (2015). In all cases, chlorine is
166 loaded above supposed saturation and Cl input can be as high as 29.1 mol.% (Table 1). The
167 mixed powder is loaded into platinum capsules (13 mm in length and 5.4 mm in diameter)
168 welded shut at both ends. The capsule is isolated from the graphite furnace with a MgO

ceramic sleeve. The intrinsic oxygen fugacities (fO_2) are supposed to be constrained by the used ¾ inch talc-Pyrex assemblies at relatively oxidizing conditions (Morizet et al. 2017) at 1.5 log unit above the Quartz-Fayalite-Magnetite (QFM) buffer.

High-pressure experiments are achieved using an end-load piston-cylinder apparatus, following the same protocol as described in Jolivet et al. (2020). Sample pressure is first increased to 0.5 GPa, then temperature is increased to ~500°C and held for 5 min for NaCl loaded syntheses, to an hour for $PdCl_2$ loaded syntheses to allow the dissociation of NaCl and $PdCl_2$, into Cl, Na and Pd, respectively. Then, pressure and temperature are increased to the final conditions. Experimental conditions for each synthesis are presented in the Table 1. We investigated a pressure range from 0.5 to 1.5 GPa, and a temperature range from 1300 to 1500°C. The temperature was monitored with a B-type thermocouple measuring at the top of the capsule. The measured temperature has a precision of ±5°C. Most of the experiment were melted for 5h. We performed an isobaric quench, using a piloted pumping system. The quench rate is at least ~100°C/s in the first 500°C.

Scanning Electron Microscopy – Energy Dispersive Spectroscopy (SEM-EDS) for major element concentrations in glasses

The chemical characterization of the recovered glasses was performed with a JEOL 5800LV SEM, equipped with a SDD SAMx EDS. The glass chips were mounted in an epoxy plug, with an ISG reference chip on each plug. We used ISG (Gin et al. 2013, Table 1), as a standard composition to ensure the correctness and robustness of the analytical measurements. The electron beam voltage was set at 15 kV and the current at 0.5 nA. The current was regularly controlled to ensure a reproducible electron flow during all the analytical campaigns. The acquisitions were conducted on a spot larger than 20 µm to avoid Na loss under the electron beam. We followed the recommendations of Newbury and Ritchie (2013)

193 to improve the quality of our results. Each sample was scanned at least 10 times with a scan
194 duration of 1 min to reduce the minimum concentration for identification (peak threshold
195 criterion, see Newburry and Ritchie 2013). We used the minor X-ray family members to
196 avoid misinterpretation near noise level and improve the quantification. We started and
197 finished all analytical measurements with 15 scans of an ISG sample to ensure there was no
198 instrumental drift. All the measurements were obtained using internal standards for the
199 different elements: LaB_6 for B_2O_3, wollastonite for SiO_2 and CaO, NaCl for Na and Cl,
200 Corundum for Al_2O_3. The EDS results were slightly corrected in accordance with the ISG
201 standard composition given by Gin et al. (2013). Based on the replicated measurements, the
202 uncertainty of the major oxide and chlorine quantification was typically ± 0.2 mol.%. All
203 chemical characterization results are shown in the Table 1.

204 **X-ray Photoelectron Spectroscopy (XPS) for chlorine speciation in glasses**

205 Several glass samples were investigated using XPS to determine the chlorine speciation.
206 Spectrum acquisition was carried out on a Kratos Nova spectrometer equipped with a
207 monochromatic Al Kα radiation operating at 1486.6 eV and 300 W. The characterization
208 (beam size 300x700 μm^2) was done on glass chips collected from the bulk of the experimental
209 charge (3x3 mm^2). We acquired the spectra with different pass energy: at 160 eV for the wide
210 spectrum with a step of 0.5 eV and at 20 eV for high-resolution XPS spectra on elements with
211 a step of 0.1 eV. The all over XPS instrument energy resolution with the pass energy 160 and
212 20 eV was on the Fermi edge 1.9 and 0.4 eV, respectively. All measurements were conducted
213 with charge neutralization owing to the insulating nature of the glass samples. The spectra
214 were referenced against the adventitious C 1s transition at 284.8 eV. For Cl species, the high-
215 resolution XPS spectra were acquired at the Cl 2p ~200 eV binding energy core level and
216 with a spectral window between 190 and 215 eV to be sufficiently large for background

subtraction and to cover the region for chloride (~199 eV) and chlorate (~208 eV) species (Moulder et al. 1992). We used the CasaXPS© software to treat the XPS spectra (Fairley et al. 2021). We used a Tougaard function for background subtraction (Tougaard 1997). For each local Cl environment, the Cl 2p peaks were fitted with two asymmetric Gaussian-Lorentzian lines linked to keep the area ratio of 1/2 between the $2p_{3/2}$ and $2p_{1/2}$ lines and a spacing of 1.6 eV in agreement with spin-orbit splitting ratio.

X-ray Absorption Spectroscopy (XAS)

For several glass samples, we acquired the Cl K-edge X-ray Absorption Spectroscopy. The acquisitions were conducted on the LUCIA beamline at SOLEIL synchrotron operating at a current of 450 mA and an energy of 2.75 GeV (Vantelon et al. 2016). Both the X-ray Absorption Near-Edge Spectroscopy (XANES) and Extended X-ray Absorption Fine Structure (EXAFS) regions were acquired. The energy of the incoming photons was selected by using double crystal monochromator Si(111). The energy calibration of the incoming photons was achieved on NaCl powder by selecting the first inflexion point of the spectrum at 2824.5 eV. The XAS spectra on the glass were collected in fluorescence mode with a silicon drift diode detector. To avoid the self-absorption effect, the geometry of the beamline was set to a low angle between the sample surface and the detector (2°).

During the experiment, the spectra were acquired with an unfocused beam having a size of 4x2 mm^2 in order to maximize the count rate. The glass powder was placed on a copper plate using carbon tape and placed inside a vacuum chamber at $5x10^{-2}$ mbar. The XAS spectra were collected at the Cl K-edge in the range 2780-3800 eV. For each point, the counting time could go up to 10 s depending on the region of interest. We collected at least five spectra on each glass sample in order to obtain an average spectrum with a good signal to noise ratio. The

presented spectra correspond to an average of the different scans for a given sample. We also conducted acquisition on several crystalline standards for comparison and fingerprinting of the XAS glass spectra: NaCl, $CaCl_2$, $PdCl_2$, $NaClO_4$. In these crystalline compounds, the Cl oxidation state varies from -1 in chlorides to +7 in perchlorates, and the local environment of Cl is changing with respect to the first coordination shell (i.e. distance and coordination number to the first neighbor).

The XAS spectra were reduced using the Demeter package; the normalization and the merge of the XAS spectra as well as the background removal were carried out with the Athena software (Newville et al. 1995; Ravel and Newville 2005) or Fastosh (Landrot 2018). In addition, the self-absorption effect was checked using the Fluo algorithm implemented in Athena. For several samples (i.e. the ones synthesized with $PdCl_2$ as the source of Cl), we had to correct the XANES spectra with the Athena deglitching package, due to the presence of several absorption peaks related to the presence of Pd and located at 3173 eV (L_3-edge) and 3330 eV (L_2-edge). The description of the spectrum treatment is provided in Suppl. Mat. 2.

The first coordination sphere to Cl atoms was obtained from the simulation of the EXAFS signal by using the single scattering signals determined by known crystalline structure: NaCl, $CaCl_2$ and $PdCl_2$, and obtained from the Crystallographic Open Database (Vaitkus et al. 2021). We used k^2-weighted signal function in the k-space between 2.85 and 8.5 $Å^{-1}$ for all spectra. The simulation of the Radial Distribution Function (RDF) using the scattering paths was done using the Artemis software. We used the spectrum from $NaClO_4$ to determine the delta E_0 (ΔE_0 = -3.8 eV) and the scattering amplitude (S_0^2 = 0.888). We used different RDF interval (1.1-3.0 Å) depending on the sample (see Table 2).

RESULTS

Cl solubility in borosilicate glasses

The recovered high-pressure glasses were examined for crystals or bubbles. Samples with strong heterogeneities were discarded from the study (i.e. samples showing phase separation). Samples with bubbles are common and kept, as the presence of bubbles assesses the saturation of chlorine in the glass. If most of the samples are transparent, several samples also exhibit a tainted brown color. For instance, the brownish color observed for C35-Cl is ascribed to the presence of tiny bubbles. We did not find Pd micro-sphere as observed in Dalou et al. (2015). We assume that most of the Pd stayed at the bottom of the capsules during the experiment, due to the way it was loaded (at the bottom instead of mixed), the high density of Pd and because of the low viscosity of borosilicate melts at >1000°C. However, as mentioned above the XAS spectra show evidence of Pd absorption peaks, which implies that some Pd is still present in the bulk glass. The content of the bubbles could not be analyzed but is assumed to be Cl_2 gas. The chlorine content in the glasses is presented in the Table 1.

We performed experiments mostly at 1 GPa and at 1400°C to focus this study on glass compositional parameters. The Cl content as a function of non-network cation concentration, expressed as the [CaO + Na_2O] is shown in Figure 1 and is obtained from the data point in Table 1. The change in Cl solubility as a function of K* as described earlier is provided in the Suppl. Mat. 2 as it turns out to be less informative than anticipated. The distinction has been made for the samples obtained with NaCl and $PdCl_2$ as the source of chlorine and as a function of pressure (0.5 to 1.5 GPa). In Figure 1, within the error in the chlorine content (±0.2 mol.%) we do not identify any effect of the initial source of chlorine. The Cl content in glasses appears strongly dependent on the non-network cation content. For instance, the lowest Cl content reached (~2 to 4 mol.%) are for the ISG composition having a low [CaO +

287 Na_2O] content; whereas the highest Cl content is observed for C35-Cl (11.1 mol.% Cl) and
288 pCABS2-Cl (~10 mol.% Cl) having high CaO content (~30 mol.%). The observed trend is not
289 surprising as Cl is thought to be incorporated in the vicinity of these cations, especially
290 alkaline-earth cations (McKeown et al. 2011, Tan 2015, Tan and Hand 2018, Zhao et al.
291 2019). The nature of the non-network forming cation should play a role as well. For instance,
292 Cl content in NH, BFS4 and BFS3 samples is increasing along with the substitution of Na for
293 Ca (see Table 1) for experiments loaded with NaCl and conducted at 1.0 GPa. The same is
294 observed for polymerized glasses such as LJ8 and BASN3: BASN3 contains only Na_2O (21.1
295 mol.%), whereas LJ8 also contains CaO (9 mol.%, plus 15.3 mol.% Na_2O), the latter is richer
296 in Cl than BASN3 of 1 to 2 mol.% (Table 1).

297 The Figure 2 presents the Cl content as a function of the XCaO defined as [CaO] / [CaO +
298 Na_2O]. The results shows that Cl content is positively correlated with the XCaO. The highest
299 Cl content is reached for the highest XCaO compositions, such as C35-Cl at 11.1 mol.% Cl
300 (XCaO = 1, see Table 1). Conversely, the lowest Cl content is observed in the Ca-free
301 compositions, such as BASN3 (from 1.1 to 3.4 mol.% Cl) and LJ4b (4 mol.% Cl, Table 1,
302 Figure 2). Compositions with similar XCaO (ISG and NH, Table 1) exhibit higher Cl content
303 when depolymerized (CaO + Na_2O content is higher). Compositions with similar K*
304 parameters, such as the NH, BFS4 and BFS3 series, solubilize more Cl with increasing
305 XCaO: 3.5 to 6.4 for NH (XCaO ~ 0.24), 6.5 for BFS4 (XCaO ~ 0.64), to 10.2 for BFS3
306 (XCaO ~ 0.83, see Table 1 and Figure 2). In lime glasses (pCABSx and C35), the Cl content
307 increases with both B_2O_3 content and CaO content, from 21.8 mol.% B_2O_3 and 16.1 mol.%
308 CaO for pCABS1-Cl, to 29.7 mol.% B_2O_3 and 26.2 mol.% CaO for C35-Cl. This is consistent
309 with the conclusion of Evans et al. (2008) and McKeown et al. (2011), which mention that Cl
310 has more affinities with Ca^{2+} in glasses than with Na^{+} cations. At first sight (from Figure 1

311 and 2), we do not observe a clear impact of the initial source of chlorine (NaCl or $PdCl_2$) on
312 the chlorine solubility, however, this aspect requires more experimental investigations to be
313 clarified.

314 **Chlorine speciation in borosilicate glasses from XPS and XANES**

315 Several glasses were characterized using Cl K-edge XAS. The Cl XANES for the studied
316 glasses and crystalline chlorine compounds are shown in Figure 3A and B, respectively. The
317 spectra for glasses have been categorized as a function of loaded chlorine source: NaCl or
318 $PdCl_2$. There is a striking feature observed in Figure 3A that is the presence of a pre-peak
319 located at ~2821 eV for the samples synthesized with $PdCl_2$ source. This peak is absent in the
320 spectra for samples synthesized with NaCl. The same pre-peak is observed in the spectrum
321 obtained for $PdCl_2$ in Figure 3B, which suggests that a non-negligible quantity of $PdCl_2$ is
322 present in the glass. Whether it corresponds to dissolved or disseminated $PdCl_2$ particles is not
323 clear and would require advanced characterization using Transmitted Electron Microscopy to
324 investigate at the nanoscale the glasses.

325 As shown in Figure 3B, there is a clear distinction between chlorine species depending on the
326 Cl oxidation state. For instance, the main line for reduced Cl in crystalline compounds (-1 in
327 NaCl, $CaCl_2$ and $PdCl_2$) is located at ~2828 eV whereas the main line for oxidized Cl in
328 crystalline compounds (+7 in $NaClO_4$) is located at ~2834 eV. The shift to higher energy in
329 the edge position is a common feature that has been documented in previous work for other
330 elements such as Fe (e.g. Wilke et al. 2011). For crystalline compounds, the main line is broad
331 in the case of NaCl and $CaCl_2$ and narrower for $NaClO_4$. The latter spectrum exhibits a broad
332 signal between 2840 and 2860 eV that is not visible in the spectra for NaCl and $CaCl_2$ or
333 $PdCl_2$. Without exception, the spectra obtained for glasses in Figure 3A show a main line

relatively broad and asymmetric with a peak maximum at 2828 eV, regardless of the initial source of chlorine and the existence of the pre-peak due to the presence of $PdCl_2$. This observation clearly indicates that chlorine is dissolved under its reduced form, Cl^-, within the glass structure and surrounded by either Na^+ or Ca^{2+} as charge balancing cation, or even Pd^{2+} in the case of samples synthesized with $PdCl_2$ as the initial source of chlorine. This result is in total agreement with the previous work using XANES from Evans et al. (2008) on aluminosilicate glasses synthesized at high pressure (0.5 GPa). McKeown et al. (2011) also pointed out that chlorine was dissolved as Cl^- with Ca^{2+} as the main balancing cation based on EXAFS simulation of the first coordination sphere for chlorine in borosilicate glasses synthesized at ambient pressure.

The suggested results from XANES analyses are confirmed by the XPS analyses that are shown in Figure 4 for several samples. The entire set of spectra is provided in the Suppl. Mat. 1. We show in Figure 4 the XPS spectra obtained in the Cl 2p energy region along with the modeling of the $2p_{3/2}$ and $2p_{1/2}$ peaks and the derived peak parameters. The nature of the chlorine source and the measured Cl content is reported on each plot. First, the nature of initial chlorine does not seem to influence the measured Cl speciation. Second, for all the characterized samples there is only one peak doublet that is ascribed to the Cl $2p_{1/2}$ and $2p_{3/2}$ located at 201 and 198 eV, respectively. The derived peak width at half maximum is on the order of 1.5 eV and the peak position are 198.7 and 200.3 eV for the Cl $2p_{3/2}$ and $2p_{1/2}$, respectively. The chlorine signal located at this binding energy corresponds to chlorine dissolved as chloride species: NaCl, $CaCl_2$ and $PdCl_2$ in our case and as reported in Moulder et al. (1992). Distinction between the chloride species is currently not possible from the spectra in Figure 4. The chloride is the only species and there is no evidence for chlorate species that would give a peak doublet between 205 and 210 eV (Moulder et al., 1992);

therefore, confirming the XANES results and in agreement with previous works on the chlorine dissolution in glasses (Evans et al. 2008, McKeown et al. 2011). Both XANES and XPS results are essential and complementary as they provide constraints on the employed model that will be used for determining the geometry of the local Cl environment in glasses using EXAFS simulation.

Chlorine local environment in borosilicate glasses from Cl K-edge EXAFS simulations

The results of the EXAFS simulations for several samples are reported in Figure 5 showing the total amplitude of the EXAFS signal ($|\chi(R)|$ in $Å^{-3}$) as a function of the RDF ($R+\Delta R$ in Å). The fitted curve to the data is shown as well as the RDF region that is of concern for the fit (see Table 2). An insert of the imaginary part ($|\chi(R)$ Img| in $Å^{-3}$) of the amplitude is also shown (the entire set of spectra is provided in Suppl. Mat. 1). It should be pointed out that the shown EXAFS spectra is corrected to remove a low RDF signal ($R+\Delta R < 1.6$ Å) that does not correspond to a chlorine signal. Details on the correction procedure is provided in Suppl. Mat. 2. Currently, we do not have any explanation for the presence of this low RDF signal. The XANES and XPS results show that chlorine dissolves as chloride species (NaCl, $CaCl_2$ and $PdCl_2$). For chlorides, the typical next nearest neighbor distance is the lowest at 2.31 Å for $PdCl_2$ (Wells et al. 1938) and is on the order of ~2.70 Å for NaCl and $CaCl_2$ (van Bever and Nieuwenkamp 1935, Finger et al. 1978). Owing to the mathematical form of the EXAFS function, such distances correspond to peak position at ~1.8 and 2.2 Å for $PdCl_2$ and NaCl or $CaCl_2$, respectively. Therefore, signals below this region do not actually correspond to a possible chlorine local environment present in the investigated borosilicate glasses. The $R+\Delta R$ signal obtained for C35-Cl is a particular case (see Figure 5E) as the signal at low radial distribution function ($R+\Delta R < 1.5$ Å) is not averaged out by the applied correction. The

peak located at ~1.4 Å could correspond to a first nearest neighbor distance close to ~1.9 Å. That distance could match adequately to the Cl-Cl distance in Cl_2 molecules (Karan and Arunan 2004). One can argue that the EXAFS signal at lower R+ΔR could also correspond to next nearest neighbor in chlorate (or perchlorate) cluster, in which a Cl^{5+} is surrounded by three oxygen atoms for charge compensation at typical distance of ~1.4 Å (Zachariasen 1929); however, we have demonstrated that chlorate species are absent from the synthesized borosilicate glasses.

The simulation of the EXAFS signal has been performed using the following single scattering paths: Cl-Na, Cl-Ca and Cl-Pd. The Cl-Pd scattering path was not used in the case NaCl was the initial source of chlorine; the Cl-Na scattering path was not used in the case of Na-free glasses (pCABS2 and C35); the Cl-Ca scattering path was not used in the case of Ca-free glasses (BASN3-212 and LJ4b). We used $r_{Cl\text{-}Na}$, $r_{Cl\text{-}Ca}$ and $r_{Cl\text{-}Pd}$ at 2.72, 2.70 and 2.31 Å. For each scattering path, we started with a Debye-Waller factor ($\sigma_{Cl\text{-}X}$) of 0.003 and fixed the coordination numbers ($CN_{Cl\text{-}X}$) at 1. The optimization of the EXAFS spectra was done with the following steps: the $r_{X\text{-}Cl}$ was optimized then followed by the $\sigma_{Cl\text{-}X}$; this step was repeated two to three times, then the $CN_{Cl\text{-}X}$ was optimized. The entire optimization procedure was repeated several times. The optimization was stopped when parameters did not show any significant improvement in the χ^2 value (χ^2 witnessing the robustness of the fit). It should be stressed that the reported simulation represents only one possible solution and that other solutions may exist.

The simulation results are provided in Table 2. The reported error bars have been determined from the Artemis software. We did not observe any systematic change of the derived parameters ($CN_{Cl\text{-}X}$, $r_{Cl\text{-}X}$ and $\sigma_{Cl\text{-}X}$) as a function of chlorine content. The derived distances to the next nearest neighbor are on average 2.29±0.13, 2.64±0.07 and 2.75±0.04 Å for Cl-Pd, Cl-

405 Na and Cl-Ca, respectively. These distances are comparable to the observed distances in
406 crystalline structures for chlorides and in good agreement with the results of Chungong et al.
407 (2017) based on neutron diffraction data. However, the obtained r_{Cl-X} distances are
408 significantly different from the results reported in McKeown et al. (2011) that extracted r_{Cl-Na}
409 close to 4 Å. The same applies to the CN_{Cl-Na} that is on the order of 8 in McKeown et al.
410 (2011) whereas it is on average 4.3 from the results in Table 2. Although it is difficult to
411 reconcile both sets of results, we point out that the proposed results in Table 2 and Figure 5
412 are a non-unique solution. The CN_{Cl-Ca} is on average 1.08 that is ¼ of the derived CN_{Cl-Na}.
413 This difference is potentially explained by the change in the cationic charge: less Ca^{2+} than
414 Na^{+} is required to charge compensate the Cl^{-}. The CN_{Cl-Na} is surprisingly high in the case of
415 NH22-2, respectively. We currently do not have any explanation for such a high CN_{Cl-Na}. One
416 hypothesis is that regions within the NH glass are enriched with respect to Na while others are
417 depleted, and Cl^{-} aggregates several Na^{+} for charge compensation. To our knowledge, these
418 results are the first obtained on the chlorine local environment in Cl-bearing borosilicate
419 glasses synthesized under high-pressure conditions; however, more advanced experimental
420 work is required to provide a full picture of the local atomic environment for chlorine
421 dissolved in glasses under different conditions: from reduced (Cl^{-}) to fully oxidized (Cl^{7+}).
422

423 **IMPLICATIONS: RATIONALE FOR CHLORINE SOLUBILITY IN**
424 **ALUMINOBOROSILICATE GLASSES**

425 Chlorine solubility results shown in the present work suggest that high-pressure conditions are
426 beneficial for dissolving large amount of chlorine in the glass. Whereas this behavior has been
427 observed for aluminosilicate glasses previously (Alletti et al. 2009, Dalou et al. 2015, Webster

et al. 2014, 2015), we also show it for aluminoborosilicate glasses with application to the immobilization of chlorine nuclear waste. It should be mentioned that the determined Cl content is higher than the I content reached in Jolivet et al. (2020) and Morizet et al. (2021a) for identical glass compositions (i.e. ISG, NH, C35), which confirms once more that there is a solubility hierarchy between halogens related to their size (Dalou et al. 2015, Dalou and Mysen 2015). In addition, chlorine solubility appears to be affected by the nature of the charge compensating cation as observed in Figure 2 and showing a strong increase in Cl solubility with increasing XCaO. This result suggests that increasing the cation charge for the Cl^- charge compensating element induces an increase in the chlorine solubility. Zhao et al. (2019) showed that changing the alkaline-earth cation also changes the chlorine solubility. These aspects imply that chlorine solubility is to some extent controlled by the nature of the charge compensating cation and that Cl^- is better dissolved in the vicinity of alkaline-earth cations.

We have synthesized this aspect in Figure 6 compiling several experimental datasets obtained on chlorine solubility. We did not gather all the existing experimental data points, however, these represents a good picture of the Cl solubility as a function of glass composition. We compiled the data 1) from Filiberto and Treiman (2009) obtained on a basaltic composition synthesized under reducing conditions; 2) from Dalou et al. (2015) investigating the effect of Al_2O_3 content on the Cl solubility in simplified Na_2O/K_2O-Al_2O_3-SiO_2 system for pressure between 0.5 and 2.5 GPa; 3) from Webster et al. (2015) that were obtained for pressure up to 0.7 GPa under oxidizing and anhydrous conditions; and 4) from the present work acquired between 0.5 and 1.5 GPa and for aluminoborosilicate glass compositions. The change in the glass composition is expressed as the Network Modifying Field Strength that is calculated with the following equation (1):

$$Net.Mod.Field\ Str. = \frac{\sum_i \frac{z_i}{r_i} \times X_i}{\sum \frac{2}{r_{O^{2-}}} \times X_{O^{2-}}} \quad (1)$$

Where X_i corresponds to the molar fraction of network modifying cation i (i.e. Na^+, K^+, Ca^{2+} and Mg^{2+} in the present database), z_i/r_i is the cation field strength defined as the ratio between the effective cationic charge divided by the cation radius. We used the data from Shannon (1976) for r_i. The dividing term is calculated from the sum of the oxygen molar fraction on network modifying oxides.

In detail, several trends or data distributions can be observed from Figure 6. The reported data points from Filiberto and Treiman (2009) at the lower right in Figure 6 suggest that imposing reducing conditions (graphite capsules corresponding to log fO_2 at QFM -1.5, Quartz-Fayalite-Magnetite buffer, relevant to martian magmatism, e.g. Herd et al. 2002) induces an observable decrease in Cl solubility. The observed lower Cl solubility under reducing conditions is comparable to the behavior observed for CO_2 (Pawley et al. 1992, Morizet et al. 2010, Wetzel et al. 2013) or S (Jugo et al. 2010, Klimm et al. 2012). The main difference is that imposing reducing experimental conditions imposes to reduce the volatile species: CO_2 reduced to CO, CH_4; S reduced to S^{2-}. It is not the case for chlorine considering that Cl^- is the most reduced chlorine species. Applying reducing conditions involve a change in the melt structure by redistributing the network modifying cations that are possibly less available for charge compensation of the negative charges for Cl^- that cannot dissolves.

The data of Dalou et al. (2015), trends on the left with increasing Al content, shows that: 1) there is a dramatic effect of the glass Al content on chlorine solubility with a maximum Cl solubility in Al-free glasses, 2) at a given composition increasing pressure induces an increase in the Cl solubility, and 3) increasing the cation field strength induces an increase in the Cl

474 solubility. The decrease in Cl solubility with increasing Al_2O_3 content can be explained by the
475 fact that Al species (i.e. AlO_4^-) in the glass require charge compensation by network
476 modifying cation due to the excess negative charge on AlO_4^- units. A comparable behavior
477 has been observed for iodine dissolved as I^- in borosilicate glasses (Jolivet et al. 2020, Morizet
478 et al. 2021b): the charge compensating cation for AlO_4^- units is not scavenged by the
479 dissolution of I^- species therefore limiting the iodine solubility. It can also be observed that
480 the Cl solubility is affected by the nature of the alkali itself and that a distinct trend in Cl
481 solubility can be observed for K-bearing and for Na-bearing glasses. We suspect that the
482 difference in the z_i/r_i between K^+ and Na^+: 0.725 and 0.980, respectively; could explain such
483 difference in Cl solubility: Increasing the z_i/r_i value would increase the Cl solubility. Our data
484 obtained on Ca-bearing glasses (Ca^{2+} with $z_i/r_i = 2$) show the highest Cl solubility above 10
485 mol.%.

486 The data from Webster et al. (2015) shown in Figure 6 exhibit an exponential increase in the
487 Cl solubility with increasing Network Modifying Field Strength, regardless of the
488 experimental conditions. Our data on aluminoborosilicate glasses also match the trend shown
489 by Webster et al. (2015) data. The glass compositions investigated in Webster et al. (2015)
490 have ~10 mol.% Al_2O_3 at the lowermost end of the Dalou et al. (2015) trends with ~11 mol.%
491 Al_2O_3. Most of the Cl solubility points are obtained on glasses having network former cation
492 concentrations (i.e. SiO_2, Al_2O_3 and B_2O_3) on the order of ~60 to 70 mol.%. C35-Cl has less
493 than 50 mol.% for SiO_2+Al_2O_3+B_2O_3 and also has the highest Cl solubility obtained.
494 Therefore, the nature and the concentration of network modifying cation appear to be of a
495 prime importance for the dissolution of chlorine. Depolymerizing the glass structure by
496 increasing the network modifying cation concentration allows the dissolution of more chlorine
497 as Cl^-. This is consistent with the high concentration of chlorine measured in natural silica

498 undersaturated rocks (Paul et al. 1976). Large interest in chlorine behavior has been raised
499 from previous experimental studies (Webster et al. 1999, 2014, 2015, 2020); however, further
500 additional work is required to build semi empirical model for chlorine solubility that can
501 integrate a broader range of glass compositions, from aluminosilicate to aluminoborosilicate
502 glasses, held under various pressure, temperature and redox conditions.

503

504 **SUMMARY**

505 In the present work, we have investigated the solubility, the speciation, and the local atomic
506 environment of chlorine in aluminoborosilicate glasses synthesized under high-pressure
507 conditions (0.5-1.5 GPa). The XPS and XANES measurements reveal that chlorine is
508 dissolved as chloride (Cl^-) species in the glass. The EXAFS fitting of the Cl spectra show that
509 the Cl^- local atomic environment is surrounded by Na^+ or Ca^{2+} at distances on the order of
510 ~2.7 Å. Furthermore, four times as much Na^+ than Ca^{2+} is required to charge compensate the
511 chloride negative charge.

512 We also show that chlorine dissolution is strongly favored in Ca-rich glass composition over
513 Na-rich ones. Comparison with previous experimental data on Cl solubility indicates that
514 describing the Cl solubility evolution as a function of glass composition is rather complex and
515 involves several aspects: 1) the nature of the Cl^- charge compensating cation, 2) the
516 concentration of Al_2O_3 that requires charge compensation, 3) the fO_2 conditions whether it is
517 oxidizing or reducing and then 4) the degree of polymerization of the glass that allows the
518 insertion of chlorine within its structure.

519

ACKNOWLEDGEMENT

The authors are grateful to the Région Pays de la Loire, which financed the current work through the Pari Scientifque "CIPress". The authors thank the Laboratoire de Planétologie et Géosciences, the Institut des Matériaux Jean Rouxel, the Nantes Université and the CNRS for providing access to the analytical facilities. We acknowledge SOLEIL for provision of synchrotron radiation facilities and we would like to thank LUCIA staff for assistance in using the beamline. We also thank Nicolas Stéphant for support on the SEM/EDS analytical platform. We would like to thank Don Baker for handling our manuscript and the two anonymous reviewers for their fruitful comments that helped to improve the quality of the manuscript.

References

Abdelouas, A., El Mendili, Y., Aït Chaou, A., Karakurt, G., Hartnack, C., Bardeau, J.-F., Saito, T., and Matsuzaki, H. (2013) A preliminary investigation of the ISG glass vapor hydration. Journal of Applied Glass Science, 4, 307-316.

Aiuppa, A., Federico, C., Giudice, G., Guerrieri, S., Paonita, A., and Valenza, M. (2004) Plume chemistry provides insights into mechanisms of sulfur and halogen degassing in basaltic volcanoes. Earth Planetary Science Letter, 222, 469–483.

Aiuppa, A., Baker, D.R., and Webster, J.D. (2009) Halogens in volcanic systems. Chemical Geology, 263, 1-18.

Alletti, M., Baker, D.R., and Freda, C. (2009) Halogen diffusion in a basaltic melt. Geochimica and Cosmochimica Acta, 71, 3570-3580.

Audi, G., and Wang, M. (2017). The NUBASE 2016 evaluation of nuclear properties. 41, 1–138.

544 Baasner, A., Schmidt, B.C., and Webb, S.L. (2013) Compositional dependence of the
545 rheology of halogen (F, Cl) bearing aluminosilicate melts. Chemical Geology, 346, 172–183.
546 van Bever, A.K., Nieuwenkamp, W. (1935) Die Kristallstruktur von Calciumchlorid, Ca Cl_2
547 Zeitschrift fuer Kristallographie, Kristallgeometrie, Kristallphysik, Kristallchemie, 90, 374-
548 376.
549 Carroll, M.R., and Webster, J.D. (1994) Solubilities of sulfur, noble gases, nitrogen, chlorine
550 and fluorine in magmas. In Volatiles in Magmas, vol. 30 (eds. M. R. Carroll and J. R.
551 Holloway). Reviews in Mineralogy, pp. 231–279.
552 Carroll, M.R. (2005) Chlorine solubility in evolved alkaline magmas. Annals of Geophysics,
553 48, 619–631.
554 Cicconi, M.R., Pili, E., Grousset, L., Florian, P., Bouillard, J.C., Vantelon, D., and Neuville,
555 D.R. (2019) Iodine solubility and speciation in glasses. Scientific Report, 9, 7758.
556 Chant, L.A., Andrews, H.R., Cornett, R.J., Koslowky, V., Milton, J.C.D., Van der Berg, J.G.,
557 Verburg, T.G., and Wolterbeek, H.T. (1996) ^{129}I and ^{36}Cl concentrations in lichens collected
558 in 1990 from three regions around Chernobyl. Applied Radiation and Isotopes, 47, 933-937.
559 Charpentier, T., Martel, L., Mir, A.H., Somers, J., Jégou, C., and Peuget, S. (2016) Self-
560 healing capacity of nuclear glass observed by NMR spectroscopy. Scientific Report, 6, 25499.
561 Chen, X., Karpukhina, N., Brauer, D.S., and Hill, R.G. (2017). High chloride content calcium
562 silicate glasses. Physical Chemistry Chemical Physics, 19(10), 7078–7085.
563 Chungong, L.F., Swansbury, L.A, Mountjoy, G., Hannon, A.C., Lee, A.F., and Martin, R.A.
564 (2017) Atomic structure of chlorine containing calcium silicate glasses by neutron diffraction
565 and ^{29}Si solid-state NMR. International journal of Applied Glass Science, 8, 383-390.

566 Collin, M., Fournier, M., Frugier, P., Charpentier, T., Moskura, M., Deng, L., Ren, M., Du, J.,
567 and Gin, S. (2018) Structure of International Simple Glass and properties of passivating layer
568 formed in circumneutral pH conditions. Nature Material Degradation, 2, 4-16.
569 Dalou, C., and Mysen, B.O. (2015) The effect of H_2O on F and Cl solubility and solution
570 mechanisms of in aluminosilicate melts at high pressure and high temperature. American
571 Mineralogist, 100, 633–643.
572 Dalou, C., Le Losq, C., Mysen, B.O., and Cody, G.D. (2015) Solubility and solution
573 mechanisms of chlorine and fluorine in aluminosilicate melts at high pressure and high
574 temperature. American Mineralogist, 100, 2272-2283.
575 Dell, W.J., Bray, P.J., and Xiao, S.Z. (1983) ^{11}B NMR studies and structural modeling of
576 Na_2O-B_2O_3-SiO_2 glasses of high soda content. Journal of Non-Crystalline Solids, 58, 1-16.
577 Dingwell, D.B., and Hess, K.-U. (1998) Melt viscosities in the system Na-Fe-Si-O-F-Cl:
578 Contrasting effects of F and Cl in alkaline melts. American Mineralogist, 83, 1016–1021.
579 Du, L.S., and Stebbins, J.F. (2005) Network connectivity in aluminoborosilicate glasses: a
580 high-resolution ^{11}B, ^{27}Al and ^{17}O NMR study. Journal of Non-Crystalline Solids, 351, 3508–
581 3520.
582 Elia A., Ferrand K., and Lemmens K. (2017) Determination of the forward dissolution rate for
583 international simple glass in alkaline solutions. MRS Advance, 12, 661-667.
584 Endt, P.M., and Van der Leun, C. (1973) Energy levels of a ¼ 21-44 nuclei (V). Nuclear
585 Physics A, 214, 1-625.
586 Evans, K.A., Mavrogenes, J.A., O'Neill, H.St.C., Keller, N.S., and Jang, L.-Y. (2008) A
587 preliminary investigation of chlorine XANES in silicate glasses. Geochemistry, Geophysics,
588 Geosystems, 9, 15 p.

589 Fairley, N., Fernandez, V., Richard-Plouet, M., Guillot-Deudon, C., Wlaton, J., Smith, E.,
590 Flahaut, D., Greiner, M., Biesinger, M., Tougaard, S., Moorgan, D., and Baltrusaitis (2021)
591 Systematic and collaborative approach to problem solving using X-ray photoelectron
592 spectroscopy. Applied Surface Science Advances, 5, 100112.
593 Filiberto, J., and Treiman, A.H. (2009) The effect of chlorine on the liquidus of basalt: First
594 results and implications for basalt genesis on Mars and Earth. Chemical Geology, 263, 60-68.
595 Finger, L.W., and King, H.E. (1978) A revised method of operation of the single-crystal
596 diamond cell and refinement of the structure of NaCl at 32 kbar. American Mineralogist, 63,
597 337-342
598 Gin, S., Abdelouas, A., Criscenti, L.J., Ebert, W.L., Ferrand, K., Geisler, T., Harrison, M.T.,
599 Inagaki, Y., Mitsui, S., Mueller, K.T., et al. (2013) An international initiative on long-term
600 behavior of high-level nuclear waste glass, Materials Today, 16, 243-248.
601 Gin, S., Jollivet, P., Tribet, M., Peuget, S., and Schuller, S. (2017). Radionuclides
602 containment in nuclear glasses: An overview. Radiochimica Acta, 105, 927–959.
603 Goel, A., McCloy, J.S., Pokorny, R., and Kruger, A.A. (2019). Challenges with vitrification
604 of Hanford High-Level Waste (HLW) to borosilicate glass – An overview. Journal of Non-
605 Crystalline Solids: X, 4, 100033.
606 Guerette M., and Huang, L. (2015) In-situ Raman and Brillouin light scattering study of the
607 international simple glass in response to temperature and pressure. Journal of Non-Crystalline
608 Solids 411, 101-105.
609 Herd, C.D.K., Borg, L.E., Jones,J.H., and Papike, J.J. (2002) Oxygen fugacity and
610 geochemical variations in the martian basalts: Implications for martian basalt petrogenesis and
611 the oxidation state of the upper mantle of Mars. Geochimica and Cosmochimica Acta, 66,
612 2025-2036.

613 Hmra, P. (2010) Retention of Halogens in Waste Glass. U.S. department of energy, Pacific
614 Northwest National Laboratory, PNNL-19361.
615 Ilyukhina, N.S., Panomaryova, I.Y., Lashchenova, T.N., and Stefanovsky, S.V. (2010).
616 Solubility of sulfate and chloride ions in borosilicate melts at vitrification of intermediate-
617 level radioactive wastes, in: WM2010 Conference, Phoenix.
618 Inagaki, Y., Kikunaga, T., Idemitsu, K., and Arima, T. (2013) Initial dissolution rate of the
619 International Simple Glass as a function of pH and temperature measured using microchannel
620 flow-through test method, Journal of Applied Glass Science, 4, 317-327.
621 Inagaki, Y. (2014) Micro-channel as a new tool to investigate glass dissolution kinetics.
622 Proceeding in Material Science, 7, 172-178.
623 Johnston, D. (1980) Volcanic contribution of chlorine to the stratosphere: More significant to
624 ozone that previously estimated? Science, 209, 491-492.
625 Jolivet, V., Jossé, L., Rivoal, M., Paris, M., Morizet, Y., Carole, L., and Suzuki-Muresan, T.
626 (2019) Quantification of boron in aluminoborosilicate glasses using Raman and ^{11}B NMR.
627 Journal of Non-Crystalline Solids, 511, 50-61.
628 Jolivet, V., Morizet, Y., Paris, M., and Suzuki-Muresan, T. (2020) High pressure experimental
629 study on iodine solution mechanisms in nuclear waste glasses, Journal of Nuclear. Materials,
630 533, 152112 .
631 Jolivet, V., Morizet, Y., Hamon, J., Paris, M., and Suzuki-Muresan, T. (2021) the influence of
632 iodide on glass transition temperature of high-pressure waste glasses. Journal of the American
633 Ceramic Society, 104, 1360-1369.
634 Jugo, P.J., Wilke, M., and Botcharnikov, R.E. (2010) Sulfur K-edge XANES analysis of
635 natural and synthetic basaltic glasses: Implications for S speciation and S content as function
636 of oxygen fugacity. Geochimica and Cosmochimica Acta, 74, 5926-5938.

637 Karan, N.K., and Arunan, E. (2004) Chlorine bond distances in ClF and Cl_2 complexes.
638 Journal of Molecular Structure, 688, 203-205.
639 Kelsey, K.E., Allwardt, J.R., and Stebbins, J.F. (2008) Ca-Mg mixing in aluminosillicate
640 glasses: an investigation using ^{17}O MAS and 3QMAS and ^{27}Al MAS NMR. Journal of Non-
641 Crystalline Solids, 354, 4644–4653.
642 Klimm, K., Kohn, S.C., O'Dell, L.A., Botcharnikov, R.E., and Smith, M.E. (2012) The
643 dissolution mechanism of sulphur in hydrous silicate melts. I: assessment of analytical
644 techniques in determining the sulphur speciation in iron-free to iron-poor glasses. Chemical
645 Geology, 322-323, 237–249.
646 Landrot G. (2018) FASTOSH: A software to process XAFS data for geochemical and
647 environmental applications. Goldschmidt Abstract, 1402.
648 Langowski, M.H., Darab, J.G., and Smith, P.A. (1996) Volatility literature of chlorine, iodine,
649 cesium, strontium, technetium, and rhenium; technetium and rhenium volatility testing. U.S.
650 department of energy, Pacific Northwest National Laboratory, PNNL-11052.
651 McKeown, D.A., Gan, H., Pegg, I.L., Stolte, W.C., and Demchenko, I.N. (2011). X-ray
652 absorption studies of chlorine valence and local environments in borosilicate waste glasses.
653 Journal of Nuclear Materials, 408, 236–245.
654 Mendoza C., Peuget S., Bouty O., Caraballo R., and Jégou C. (2012) Simplified nuclear
655 glasses structure behaviour under various irradiation conditions: a Raman spectroscopy study.
656 Proceeding in Chemistry, 7, 581-586.
657 Méplan, O., and Nuttin A. (2006) La gestion des déchets nucléaires. Images de la Physique, 9-
658 17.
659 Metcalfe, B.L., and Donald, I.W. (2004) Candidate wasteforms for the immobilization of
660 chloride-containing radioactive waste. Journal of Non-Crystalline Solids, 348, 225–229.

661 Métrich, N., and Rutherford, M.J. (1992) Experimental study of chlorine behavior in hydrous
662 silicic melts. Geochimica and Cosmochimica Acta, 56, 607–616.
663 Mohd Fadzil, S., Hrma P., Schweiger M.J., and Riley B.J. (2015) Liquidus temperature and
664 chemical durability of selected glasses to immobilize rare earth oxides waste. Journal of
665 Nuclear Materials, 465, 657-663.
666 Morizet, Y., Paris, M., Gaillard, F., and Scaillet, B. (2010) C-O-H fluid solubility in
667 haplobasalt under reducing conditions: an experimental study. Chemical Geology, 279, 1–16.
668 Morizet, Y., Paris, M., Sifré, D., Di Carlo, I., Ory, S., and Gaillard, F. (2017) Towards the
669 reconciliation of viscosity change and CO_2-induced polymerization in silicate melts. Chemical
670 Geology, 458, 38-47.
671 Morizet, Y., Hamon, J., La, C., Jolivet, V., Suzuki-Muresan, T., and Paris, M. (2021a)
672 Immobilization of ^{129}I in nuclear waste glass matrixes synthesized under high-pressure
673 conditions: an experimental study. Journal of Materials Chemistry A, 9, 23902.
674 Morizet, Y., Jolivet, V., Trcera, N., Suzuki-Muresan, T., and Hamon, J. (2021b) Iodine local
675 environment in high pressure borosilicate glasses: An X-ray photoelectron spectroscopy and
676 X-ray absorption spectroscopy investigation. Journal of Nuclear Materials, 553, 153050.
677 Moulder, J.F., Stickle, W.F., Sobol, P.E., and Bomben, K.D. (1992) Handbook of W-ray
678 Photo- electron Spectroscopy: a reference book of standard spectra for identification and
679 interpretation of XPS spectra, J. Chastain Ed., Perkin-Elmer Corporation Physical Electronics
680 Division, Eden Prairie, Minnesota.
681 Newbury, D.E., and Ritchie, N.W.M. (2013) Is scanning electron microscopy/energy
682 dispersive X-ray spectrometry (SEM/EDS) quantitative? Scanning, 35, 141-168.
683 Newville, M., Ravel, B., Haskel, D., Rehr, J.J., Stern, E.A., and Yacoby, Y. (1995) Analysis
684 of multiple-scattering XAFS data using theoretical standards. Physica B, 208/209, 154–156.

685 Ojovan, M.I., and Lee, W.E. (2011) Glassy wasteforms for nuclear waste immobilization.
686 Metallurgical and Materials Transactions A: Physical Metallurgy and Materials Science, 42,
687 837–851.
688 Paul, D.K., Buckley, F., and Nixon, P.H. (1976) Fluorine and chlorine geochemistry of
689 kimberlites. Chemical Geology, 17, 125-133.
690 Pawley, A.R., Holloway, J.R., and McMillan, P.F. (1992) The effect of oxygen fugacity on
691 the solubility of carbon–oxygen fluids in basaltic melt. Earth Planetary Science Letter, 110,
692 213–225.
693 Ravel, B., and Newville, M. (2005) ATHENA, ARTHEMIS, HEPHAESTUS: data analysis
694 for Xray absorption spectroscopy using IFEFFIT. Journal of Synchrotron Radiation, 12, 537–
695 541.
696 Riley, B.J., Vienna, J.D., Strachan, D.M., McCloy, J.S., and Jerden Jr., J.L. (2016) Materials
697 and processes for the effective capture and immobilization of radioiodine: a review. Journal of
698 Nuclear Materials, 470, 307–326.
699 Roux, C., Le Gal La Salle, C., Simonucci, C., Van Meir, N., Fifield, L. K., Bourlès, D. L., and
700 Lancelot, J. (2014) High ^{36}Cl/Cl ratios in Chernobyl groundwater. Journal of Environmental
701 Radioactivity, 138, 19–32.
702 Schofield, J.M., Bingham, P.A., and Hand, R.J. (2009) The immobilisation of a chloride
703 containing actinide waste surrogate in calcium aluminosilicate glasses, in: A. Cozzi, T. Ohji
704 (Eds.), Environmental Issues and Waste Management Technologies in the Materials and
705 Nuclear Industries XII, John Wiley & Sons, Inc, pp. 69-80.
706 Shannon, R.D. (1976) Revised effective ionic radii and systematic studies of interatomic
707 distances in halides and chalcogenides. Acta Crystallographia, A32, 751-767.

708 Signorelli, S., and Carroll, M.R. (2002) Experimental study of Cl solubility in hydrous
709 alkaline melts: constraints on the theoretical maximum amount of Cl in trachytic and
710 phonolitic melts. Contribution to Mineralogy and Petrology, 143, 209–218.
711 Siwadamrongpong, S., Koide, M., and Matusita, K. (2004) Prediction of chloride solubility in
712 CaO-Al_2O_3-SiO_2 glass systems. Journal of Non-Crystalline Solids, 347, 114–120.
713 Symonds, R.B., Rose, W.I., and Reed, M.H. (1988) Contribution of Cl- and F-bearing gases
714 to the atmosphere by volcanoes, Nature, 334, 415-418.
715 Tan, S. (2015). The incorporation and solubility of sulphate, chloride and molybdate anions in
716 borosilicate and aluminosilicate glasses. Immobilisation Science Laboratory, pp. 254.
717 Tan, S., and Hand, R.J. (2018) Incorporation and phase separation of Cl in alkaline earth
718 aluminosilicate glasses. Journal of Nuclear Materials, 507, 135–144.
719 Thomas, R.W., and Wood, B.J. (2021) The chemical behaviour of chlorine in silicate melts.
720 Geochimica et Cosmochimica Acta, 294, 28–42.
721 Tomilin, S.V., Lukinykh, A.N., Lizin, A.A., Bychkov, A.V., Yakovlev, V.V., and Konovalov,
722 V.I. (2007) Investigation of the incorporation of spent alkali chloride melt in ceramic. Atomic
723 Energy, 102, 217–222.
724 Tougaard, S. (1997) Universality classes of inelastic electron scattering cross-sections.
725 Surface Interface Analysis, 25, 137–154.
726 Vaitkus, A., Merkys, A., and Grazulis, S. (2021) Validation of the Crystallographic Open
727 Database using the Crystallographic Information Framework. Journal of Applied
728 Crystallography, 54, 661-672.
729 Vance, E.R., Davis, J., Olufson, K., Chironi, I., Karatchevtseva, I., and Farnan, I. (2012)
730 Candidate waste forms for immobilisation of waste chloride salt from pyroprocessing of spent
731 nuclear fuel. Journal of Nuclear Materials, 420, 396–404.

732 Vantelon, D., Trcera, N., Roy, D., Moreno, T., Mailly, D., Guillet, S., Metchalkov, E.,
733 Delmotte, F., Lassalle, B., Lagarde, P., and Flank, A.M. (2016) The LUCIA beamline at
734 SOLEIL. Journal of Synchrotron Radiation, 23, 635–640 .
735 Webster, J.D., Kinzler, R.J., and Mathez, A. (1999) Chloride and water solubility in basalt
736 and andesite melts and implications for magmatic degassing. Geochimica and Cosmochimica
737 Acta, 63, 729-738.
738 Webster, J. D., Goldoff, B., Sintoni, M. F., Shimizu, N., and De Vivo, B. (2014) C-O-H-Cl-S-
739 F volatile solubilities, partitioning, and mixing in phonolitic trachytic melts and aqueous-
740 carbonic vapor ± saline liquid at 200 MPa. Journal of Petrology, 55, 2217–2248.
741 Webster, J.D., Vetere, F., Botcharnikov, R.E., Goldoff, B., McBirney, A., and Doherty, A.L.
742 (2015) Experimental and modeled chlorine solubilities in aluminosilicate melts at 1 to 7000
743 bars and 700 to 1250 °C: Applications to magmas of Augustine Volcano, Alaska. American
744 Mineralogist, 100, 522–535.
745 Webster, J.D., Baker, D.R., and Aiuppa, A. (2018) Halogens in mafic and intermediate-silica
746 content magmas. In: Harlov D., Aranovich L.Y. (Eds.), The Role of Halogens in Terrestrial
747 and Extraterrestrial Geochemical Processes: Surface, Crust and Mantle. Springer Lectures in
748 Geology Series, pp. 307–430.
749 Webster, J.D., Iveson, A.A., Rowe, M.C., and Webster, P.M. (2020) Chlorine and felsic
750 magma evolution: Modelling the behavior of an under-appreciated volatile component.
751 Geochimica and Cosmochimica Acta, 271, 248-288.
752 Wells, A.F. (1938) The Crystal Structure of Palladous Chloride $PdCl_2$. Zeitschrift fuer
753 Kristallographie, Kristallgeometrie, Kristallphysik, Kristallchemie, 100, 189-194.

754 Wetzel, D.T., Rutherford, M.J., Jacobsen, S.D., Hauri, E.H., and Saal, A.E. (2013) Degassing
755 of reduced carbon from planetary basalts. Proceedings of the National Academy of Science,
756 110, 8010-8013.
757 Wickham, A., Steinmetz, H.J., O'Sullivan, P., and Ojovan, M.I. (2017). Updating irradiated
758 graphite disposal: Project 'GRAPA' and the international decommissioning network. Journal
759 of Environmental Radioactivity, 171, 34–40.
760 Wilke, M., Klimm, K., and Kohn, S.C. (2011) Spectroscopic studies on sulfur speciation in
761 synthetic and natural glasses. In H. Behrens and J.D. Webster, Eds., Sulfur in Magmas and
762 Melts: Its Importance for Natural and Technical Processes, 73, p. 41–78. Reviews in
763 Mineralogy and Geochemistry, Mineralogical Society of America, Chantilly, Virginia.
764 Zhao, W., Li, K., Lin, P., Xu, K., and Tan, S. (2019) Dissolution of Cl in alkaline earth (Ca,
765 Sr, Ba) aluminosilicate glasses. Journal of Non-Crystalline Solids, 516, 56–62.
766 Zachariasen, W.H. (1929) The Crystal Structure of Sodium Chlorate. Zeitschrift fuer
767 Kristallographie, Kristallgeometrie, Kristallphysik, Kristallchemie, 71, 517-529.
768 Zimova, M., and Webb, S.L. (2007) The combined effects of chlorine and fluorine on the
769 viscosity of aluminosilicate melts. Geochimica et Cosmochimica Acta, 71, 1553–1562.
770

771 **Figure caption**

772 Figure 1: Chlorine content as a function of non-network former cations content expressed as
773 the [CaO + Na_2O] showing the gradual increase in Cl solubility with increasing network
774 modifying cation concentration.
775 Figure 2: Change in Cl solubility as a function of XCaO = [CaO] / [CaO + Na_2O]. It can be
776 clearly observed that Cl solubility is enhanced in the case of Ca-rich glasses in comparison to
777 Na-rich suggesting that the nature of the cation itself plays a major role on Cl solubility.

778 Figure 3: Cl K-edge XANES spectra acquired for glasses (A) and crystalline compounds (B).
779 The used source of chlorine is indicated for Cl-bearing glasses.
780 Figure 4: XPS spectra in the Cl 2p binding energy region and obtained for several glasses
781 with different Cl content up to 11.1 mol.%. Chlorine is dissolved only as chloride species as
782 witnessed by the doublet peak located at ~200 eV. The peak fitting parameters are indicated
783 next to each simulation. There is no evidence of chlorate species.
784 Figure 5: Radial Distribution Function (R+ΔR in Å) obtained from EXAFS spectra for glasses
785 with different Cl content. The insert corresponds to the imaginary part of the RDF amplitude
786 spectrum. The fitted region is indicated and does not consider the lower R+ΔR signal that is
787 considered as an unwanted EXAFS signal and basically filtered (see Suppl. Mat. 2).
788 Figure 6: Chlorine solubility (in mol.%) as a function of the Network Modifying Field
789 Strength (see text for the detailed calculation). Along to this work, several other datasets are
790 also reported: Filiberto and Treiman (2009), Dalou et al. (2015), Webster et al. (2015). The
791 trends in the data of Dalou et al. (2015) is ascribed to the difference in the Al_2O_3 content; the
792 lower chlorine solubility for Filiberto and Treiman (2009) can be explained by the reducing
793 conditions applied during their experiments.

Table 1: Experimental conditions, major element concentrations and chlorine solubility in synthesized glasses.

Sample	T (°C)	P (GPa)	Duration (h)	$Cl^{init.d}$	SiO_2	Al_2O_3	B_2O_3	CaO	Na_2O	ZrO_2	Total	$Cl^{sol.}$	K*[a]	R*[a]	XCaO[b]	NMFS[c]
					Mol.%[e]											
ISG21-1 $PdCl_2$	1400	0.5	5	11.4	64.6	4.0	17.5	4.5	5.2	1.9	97.7	2.3	3.9	0.6	0.46	1.70
ISG21-2 $PdCl_2$	1400	0.5	5	27.2	60.0	3.8	16.9	5.6	8.7	1.8	96.7	3.3	3.8	0.3	0.39	1.74
ISG22-1 $PdCl_2$	1400	1	5	17.1	64.6	4.0	17.8	4.0	5.1	2.0	97.5	2.5	3.9	0.5	0.44	1.70
ISG22-2 $PdCl_2$	1400	1	5	29.1	61.5	3.8	16.9	5.0	7.5	2.0	96.8	3.2	3.9	0.3	0.4	1.72
ISG23-1 $PdCl_2$	1400	1.5	5	15.6	63.1	4.0	18.6	4.4	5.2	2.0	97.3	2.7	3.6	0.6	0.46	1.72
ISG23-2 $PdCl_2$	1400	1.5	5	22.3	61.2	3.8	16.4	5.2	7.8	2.0	96.4	3.6	4.0	1.0	0.4	1.72
ISG22-1 NaCl	1400	1	5	4.4	57.1	3.6	15.2	5.5	13.7	1.6	96.6	3.4	4.0	1.0	0.29	1.78
ISG22-2 NaCl	1400	1	5	6.5	57.0	3.6	15.2	5.4	13.7	1.6	96.5	3.5	4.0	1.0	0.28	1.78
ISG22-3 NaCl	1400	1	5	11.3	56.9	3.6	15.3	5.4	13.7	1.5	96.4	3.6	4.0	3.2	0.28	1.78
LJ8 221 NaCl	1400	1	5	3.5	62.3	6.0	5.4	7.9	15.6		97.1	2.9	12.7	2.7	0.34	1.70
LJ8 222 NaCl	1400	1	5	6.9	61.1	5.8	6.0	7.8	15.5		96.2	3.8	11.2	2.8	0.33	1.71
LJ8 021 NaCl	1200	1	1	6.5	60.5	5.4	6.7	8.0	15.2		95.8	4.2	9.9	2.8	0.34	1.71
BASN3-211 NaCl	1400	0.5	4	3.8	62.4	9.8	4.4		22.3		98.9	1.1	16.2	3.1	0	1.81
BASN3-212 NaCl	1400	0.5	4	11.5	62.3	9.8	4.4		22.3		98.9	1.1	16.2	3.6	0	1.81
BASN3 221 NaCl	1400	1	5	3.8	61.6	9.7	4.4		23.0		98.7	1.3	16.1	3.3	0	1.82
BASN3 223 NaCl	1400	1	5	11.5	61.3	9.6	4.4		23.3		98.6	1.4	16.0	1.6	0	1.82
BASN3-231 NaCl	1400	1.5	4	3.8	63.7	9.7	3.1		20.8		97.4	2.6	23.4	0.9	0	1.78
BASN3-232 NaCl	1400	1.5	4	11.5	63.2	9.1	3.7		21.2		97.3	2.7	19.7	0.4	0	1.79
BASN3-021 NaCl	1200	1	1	6.3	61.6	8.2	7.2		19.6		96.6	3.4	9.6	0.8	0	1.80
NH21-1 $PdCl_2$	1400	0.5	5	13.3	46.0	9.8	15.9	7.9	16.9		96.5	3.5	3.5	1.8	0.32	1.92
NH21-2 $PdCl_2$	1400	0.5	5	24.6	55.5	9.0	15.6	6.4	9.6		96.2	3.8	4.1	1.7	0.4	1.81
NH22-1 $PdCl_2$	1400	1	5	13.7	49.4	10.5	13.5	7.8	13.3		94.5	5.5	4.4	2.1	0.37	1.86
NH22-2 $PdCl_2$	1400	1	5	26.3	44.7	9.5	13.5	7.7	18.7		94.0	6.0	4.0	2.0	0.29	1.92
NH22-2 NaCl	1400	1	5	7.3	40.9	9.0	13.4	7.6	25.5		96.4	3.6	3.7	0.5	0.23	1.99
NH22-3 NaCl	1400	1	5	12.0	39.0	8.8	13.7	7.0	25.1		93.6	6.4	3.5	1.7	0.22	2.01
BFS3-222 NaCl	1400	1	5	11.7	41.1	5.4	12.4	25.6	5.3		89.8	10.2	3.8	0.7	0.83	1.69
BFS4-221 NaCl	1400	1	5	7.7	46.1	6.0	11.8	18.9	10.7		93.5	6.5	4.4	0.5	0.64	1.75
pCABS1-Cl $PdCl_2$	1350	1	4	15.2	50.6	5.5	21.8	16.1			94.0	6.1	2.6	0.6	1	1.74
pCABS2-Cl $PdCl_2$	1350	1	4	10.0	44.5	5.1	13.4	27.4			90.4	9.6	3.7	0.5	1	1.63
C35-Cl $PdCl_2$	1350	1	4	14.5	28.2	4.8	29.7	26.2			88.9	11.1	1.1	0.6	1	1.87
LJ4b-223 NaCl	1400	1	5	11.4	48.1		31.3		16.6		96.0	4.0	1.5	1.0	0	1.98

[a] The K* and R* parameters are derived from the parameters defined by Dell et al. (1983) for Na-bearing borosilicate glasses and have been modified in order to introduce the presence of Al_2O_3 and the presence of CaO. See text for the details on the calculations.

[b] The XCaO is defined as the ratio between CaO and the total network modifying cation concentration such as [CaO] / [CaO + Na_2O].

[c] The NMFS corresponds to the Network Modifying Field Strength that is calculated from Eq. 1. It stands for the field strength (z_i/r_i) of the network modifying cations (Ca^{2+} and Na^{+}) normalized to the field strength of the total oxygen carried by the network modifying cations.

[d] The $Cl^{init.}$ indicates the initial loaded chlorine content in the capsule either as NaCl or $PdCl_2$.

[e] The major element concentrations including the chlorine solubility have been determined using SEM-EDS and the B_2O_3 content is calculated from the total and corrected according to the ISG standard (see Jolivet et al. 2020). The typical error bar on each oxide and chlorine is ±0.2 mol.%.

Table 2: Cl K-edge EXAFS spectra simulation results for chlorine local atomic environment in glasses.

Sample	$Cl^{sol.}$	R space (Å)[a]	CN_{Cl-Pd}	r_{Cl-Pd}	s_{Cl-Pd}	CN_{Cl-Na}	r_{Cl-Na}	s_{Cl-Na}	CN_{Cl-Ca}	r_{Cl-Ca}	s_{Cl-Ca}
LJ4b-223	4.0	1.5-2.8				2.46(14)[b]	2.70(0)	0.012(1)			
BASN3-212	1.1	1.5-2.8				3.63(26)	2.67(1)	0.023(1)			
BFS3-222[d]	10.2	1.75-2.9				0.44(14)	2.52(2)	0.007(4)	0.68(17)	2.77(2)	0.015(4)
ISG23-2	3.6	1.1-3.0	1.97(6)	2.30(0)	0.012(0)	5.91(32)	2.68(1)	0.036(1)	0.63(5)	2.74(1)	0.008(1)
NH22-2 $PdCl_2$	6.0	1.7-3.0	0.42(9)	2.15(2)	0.014(2)	8.86(88)	2.64(3)	0.076(6)	0.40(4)	2.80(1)	0.001(0)
pCABS2-Cl	9.6	1.75-2.8	0.72(20)	2.46(3)	0.023(4)				1.73(11)	2.72(1)	0.017(1)
C35-Cl[c]	11.1	1.75-2.8	0.51(15)	2.23(2)	0.016(4)				1.95(16)	2.70(1)	0.018(1)

[a] The R space corresponds to the Radial Distribution Function interval obtained from EXAFS that has been fitted.
[b] The error derived on each fitted parameter is reported in between the brackets and corresponds to a variation on the last digit value. The error has been from the Artemis fitting software.
[c] For this particular sample, we observe a strong signal not averaged out by the R background (see Suppl. Mat.) located at ~1.3 Å, which could correspond to a distance to first neighbor on the order of ~1.8 Å. Although, we did not try to simulate this peak we ascribe it to the possible presence of bubbles filled with gaseous Cl_2 with r_{Cl-Cl} = 1.8 Å.
[d] The reported data for this sample is uncertain considering the possibility for Na^+ and Ca^{2+} to be in the vicinity of the Cl^- species. Hence, the simulations using either Cl-Na path or Cl-Ca path or both Cl-Na and Cl-Ca paths lead to very similar results. In other words, the distinction between the Ca or Na local environments surrounding the Cl^- is not possible.

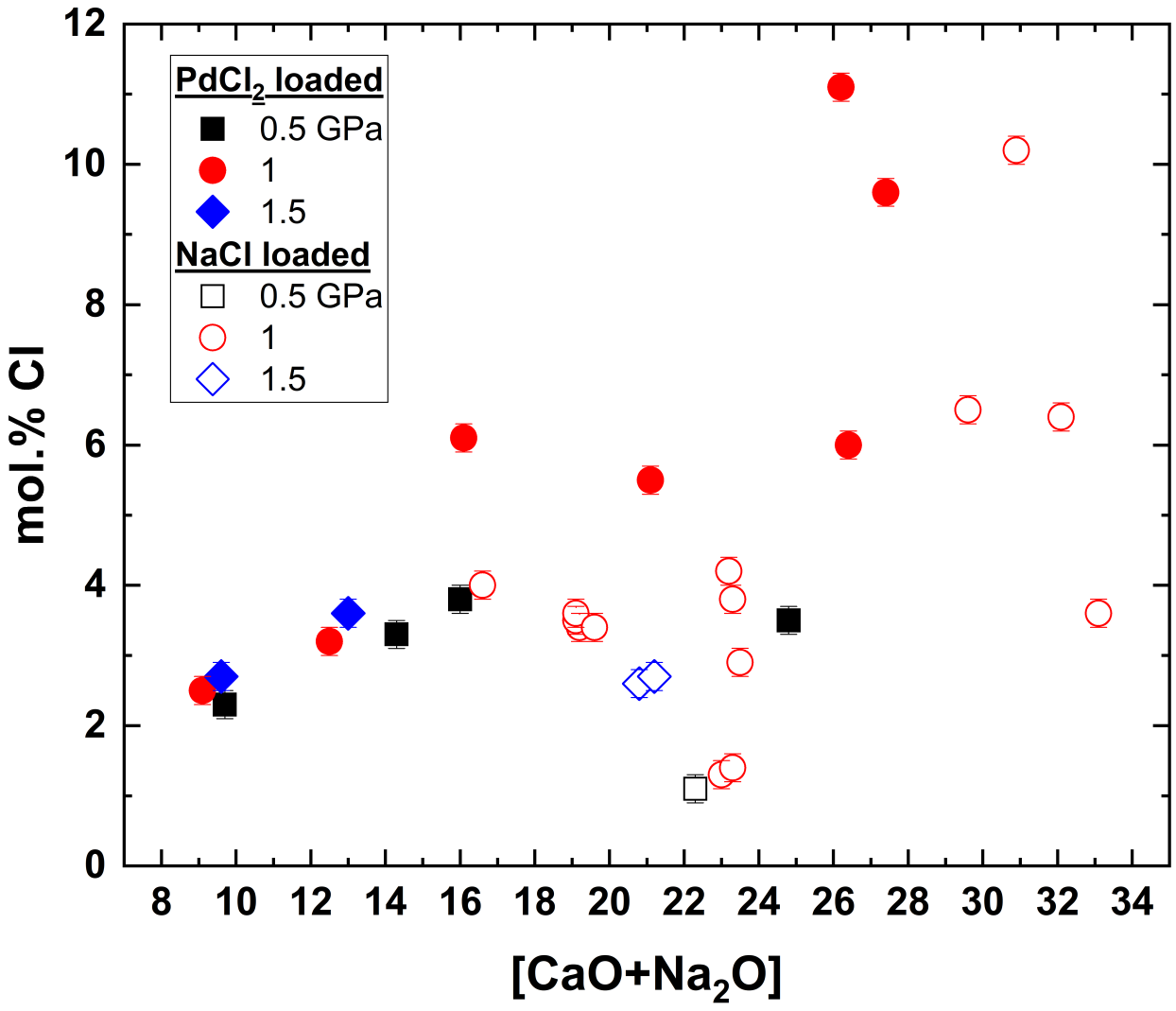
PdCl2 loaded
0.5 GPa
1
1.5
NaCl loaded
0.5 GPa
1
1.5
mol.% Cl
[CaO+Na2O]
0
2
4
6
8
10
12
8
10
12
14
16
18
20
22
24
26
28
30
32
34

Figure 1

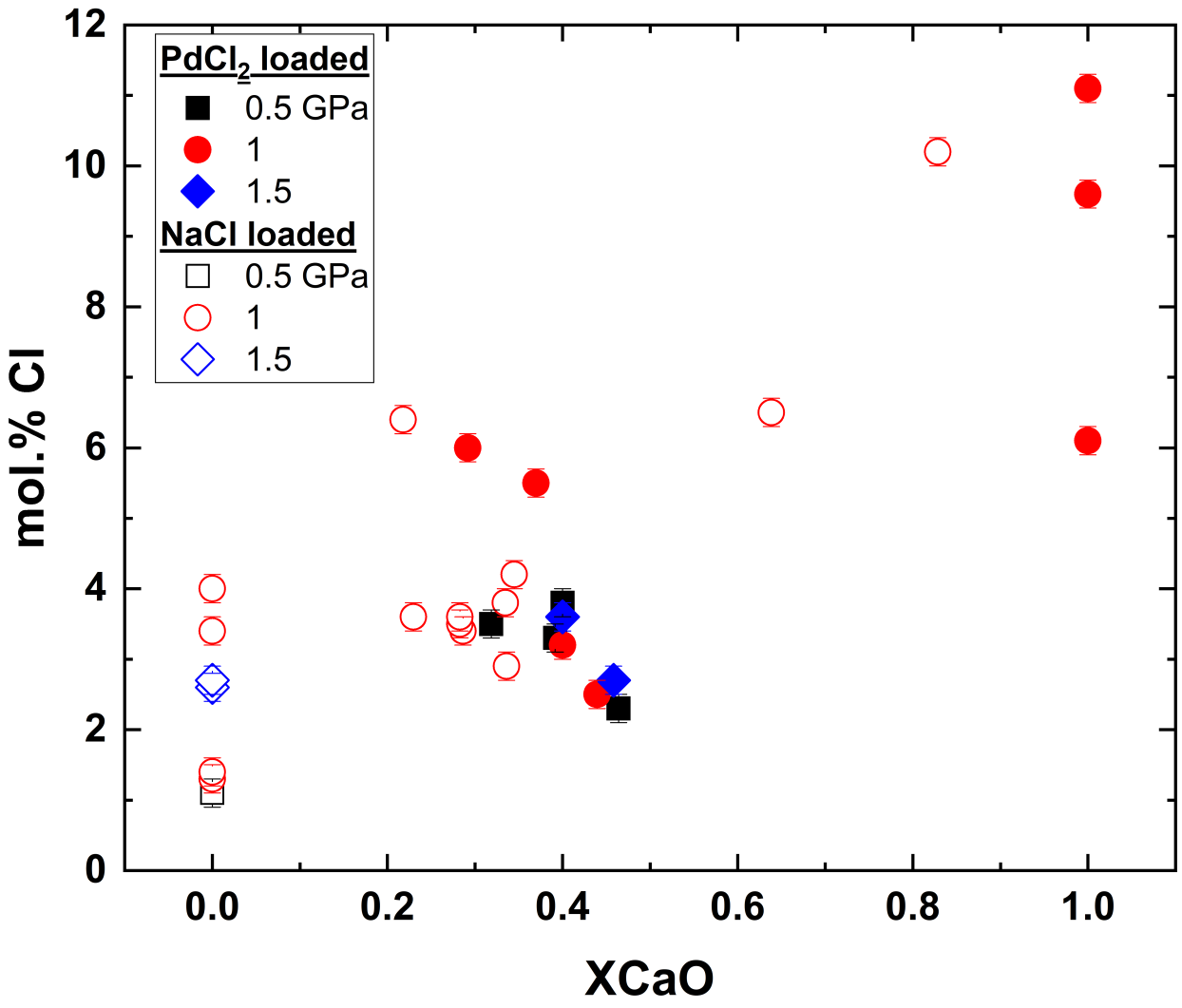
PdCl2 loaded
0.5 GPa
1
1.5
NaCl loaded
0.5 GPa
1
1.5
mol.% Cl
XCaO
0
2
4
6
8
10
12
0.0
0.2
0.4
0.6
0.8
1.0

Figure 2

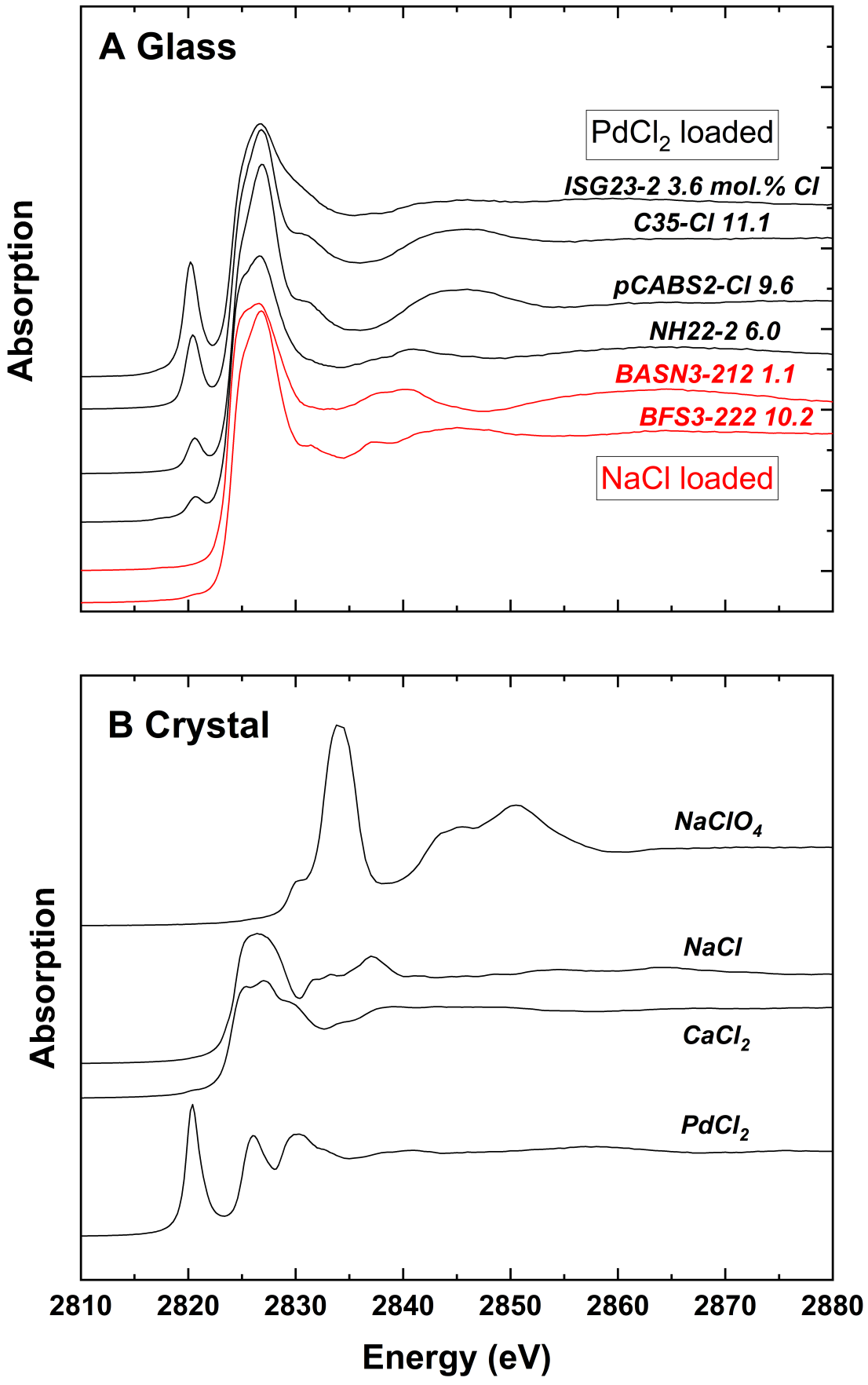
A Glass
PdCl2 loaded
ISG23-2 3.6 mol.% Cl
C35-Cl 11.1
pCABS2-Cl 9.6
NH22-2 6.0
BASN3-212 1.1
BFS3-222 10.2
NaCl loaded
Absorption
B Crystal
NaClO4
NaCl
CaCl2
PdCl2
Absorption
2810
2820
2830
2840
2850
2860
2870
2880
Energy (eV)

Figure 3

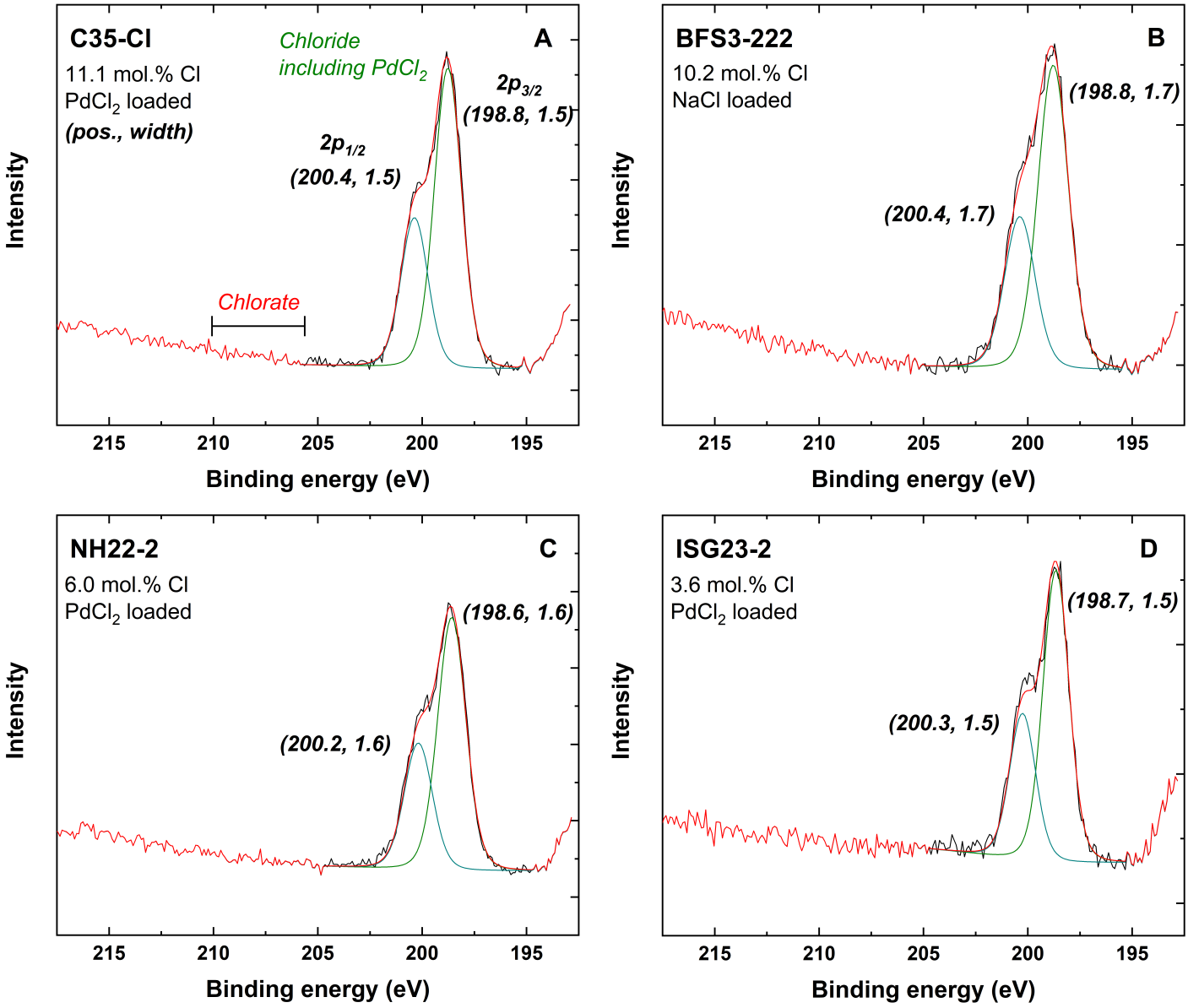
C35-Cl
11.1 mol.% Cl
PdCl2 loaded
(pos., width)
Chloride
including PdCl2
A
2p3/2
(198.8, 1.5)
2p1/2
(200.4, 1.5)
Chlorate
Intensity
215
210
205
200
195
Binding energy (eV)
BFS3-222
10.2 mol.% Cl
NaCl loaded
B
(198.8, 1.7)
(200.4, 1.7)
NH22-2
6.0 mol.% Cl
PdCl2 loaded
C
(198.6, 1.6)
(200.2, 1.6)
ISG23-2
3.6 mol.% Cl
PdCl2 loaded
D
(198.7, 1.5)
(200.3, 1.5)

Figure 4

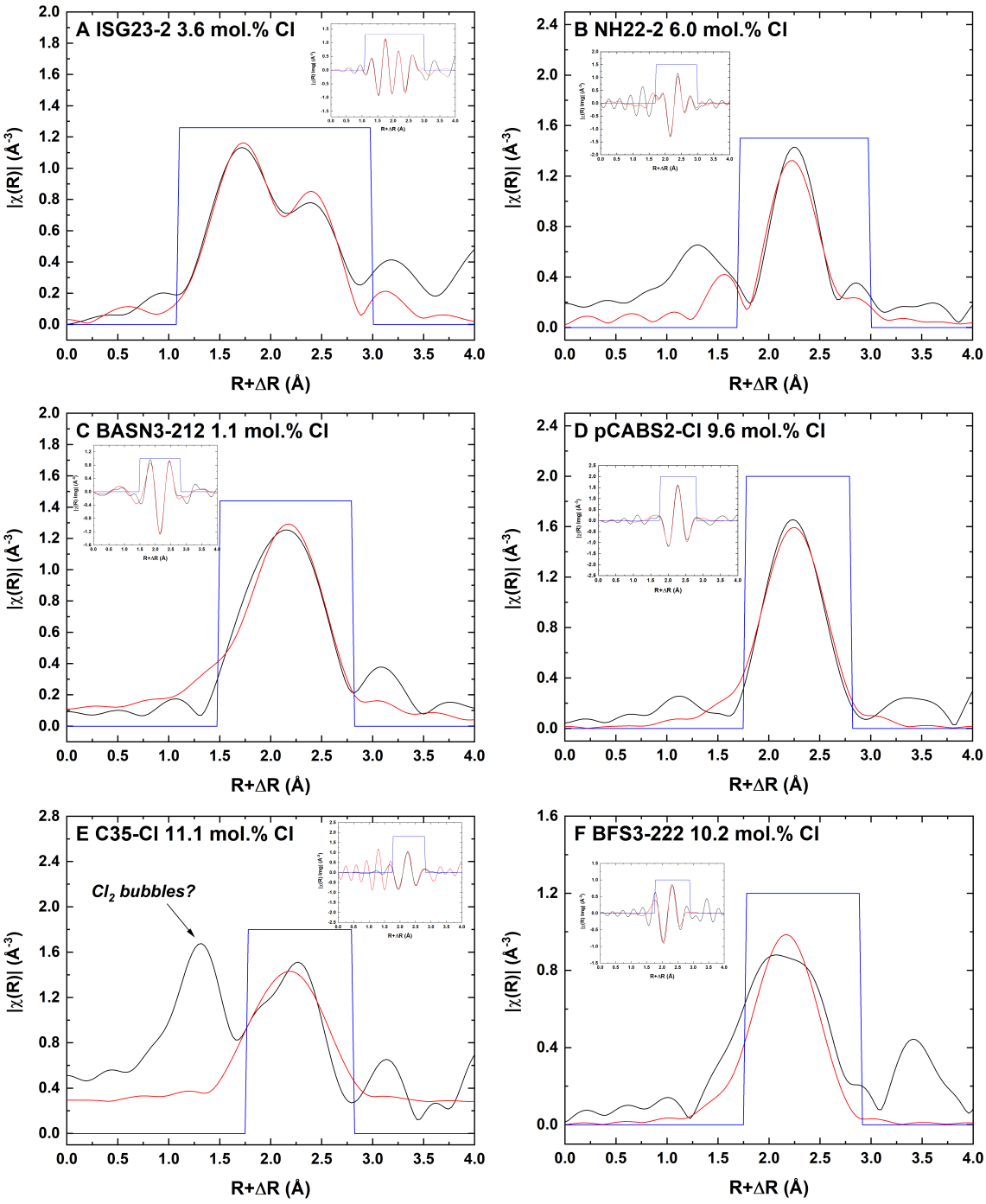
A ISG23-2 3.6 mol.% Cl
B NH22-2 6.0 mol.% Cl
C BASN3-212 1.1 mol.% Cl
D pCABS2-Cl 9.6 mol.% Cl
E C35-Cl 11.1 mol.% Cl
Cl2 bubbles?
F BFS3-222 10.2 mol.% Cl
|χ(R)| (Å-3)
R+ΔR (Å)

Figure 5

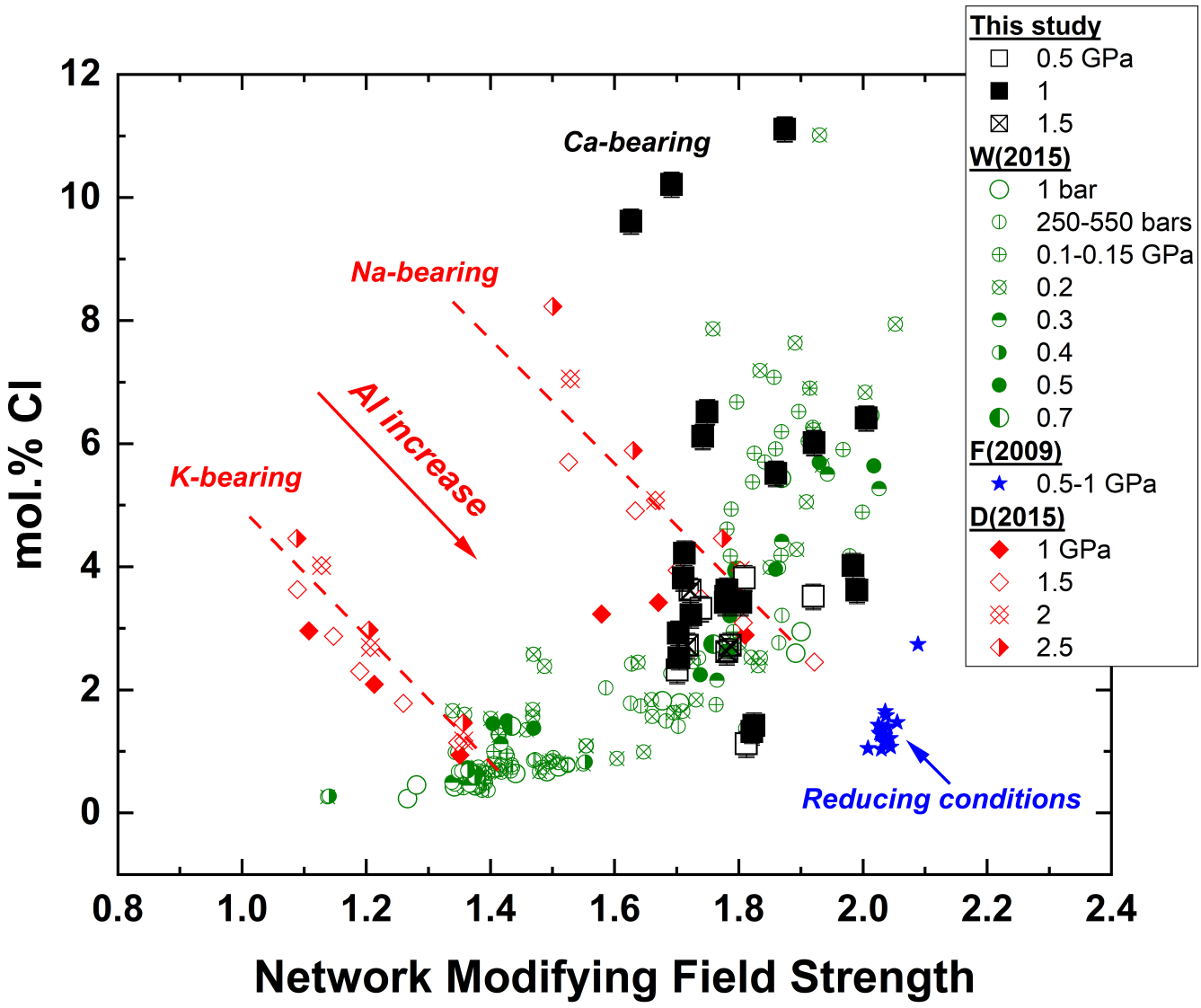
This study
0.5 GPa
1
1.5
W(2015)
1 bar
250-550 bars
0.1-0.15 GPa
0.2
0.3
0.4
0.5
0.7
F(2009)
0.5-1 GPa
D(2015)
1 GPa
1.5
2
2.5
Ca-bearing
Na-bearing
K-bearing
Al increase
Reducing conditions
mol.% Cl
Network Modifying Field Strength
0
2
4
6
8
10
12
0.8
1.0
1.2
1.4
1.6
1.8
2.0
2.2
2.4

Figure 6